



Contents lists available at ScienceDirect

Remote Sensing of Environment

journal homepage: www.elsevier.com/locate/rse

Small anomalies in dry-season greenness and chlorophyll fluorescence for Amazon moist tropical forests during El Niño and La Niña

Russell Doughty^{a,b}, Xiangming Xiao^{a,*}, Yuanwei Qin^a, Xiaocui Wu^a, Yao Zhang^c, Berrien Moore III^d

^a Department of Microbiology and Plant Biology, University of Oklahoma, Norman, OK 73019, United States of America

^b Division of Geological and Planetary Sciences, California Institute of Technology, Pasadena, CA, United States of America

^c Department of Environmental Science, Policy and Management, University of California Berkeley, Berkeley, CA, 94720, United States of America

^d College of Atmospheric and Geographic Sciences, University of Oklahoma, Norman, OK 73019, United States of America

ARTICLE INFO

Keywords:

Solar-induced chlorophyll fluorescence
Gross primary productivity
Drought
El Niño–southern oscillation
MODIS
GOME-2
OCO-2
MAIAC

ABSTRACT

The Amazon Basin, a major driver of atmospheric CO₂ fluxes, is composed of moist tropical forest (> 2000 mm mean annual precipitation), seasonally moist tropical forests (< 2000 mm mean annual precipitation), croplands, and pastures. It is debated whether there is a dry-season increase in photosynthesis for moist forest and a large reduction in photosynthesis of tropical South America was recently cited as a major driver of the historically high atmospheric CO₂ growth rate during the 2015/2016 El Niño. To address this debate and to gain insight into changes in dry-season greenness, SIF, and photosynthesis during El Niño–Southern Oscillation (ENSO) events, here we investigate (1) dry-season changes in satellite-based greenness, solar-induced chlorophyll fluorescence (SIF), and photosynthesis during 2007–2017 and (2) anomalies of satellite-based dry-season greenness, SIF, and photosynthesis for two El Niño events (2009/2010 and 2015/2016) and two La Niña events (2007/2008 and 2010/2011). We hypothesize that satellite-based greenness, SIF, and photosynthesis of moist tropical forests should increase during the dry season, and find this to be the case using two MODIS BRDF-adjusted vegetation indices (EVI and NDVI), GOME-2 SIF data, and the Vegetation Photosynthesis Model (VPM). We also hypothesize that dry-season greenness, SIF, and photosynthesis should be anomalously high during the El Niños, due to anomalously high photosynthetically active radiation (PAR) and a relatively normal preceding wet season, and anomalously low during the La Niñas because these dry seasons were preceded by anomalously low amounts of wet-season precipitation. For this hypothesis, we present results for moist tropical forest and at the basin scale to determine if and by how much their anomalies differ. We find dry-season greenness, SIF, and photosynthesis of moist tropical forest and at the basin scale were statistically significantly lower than normal during the La Niñas, significantly higher than normal during the 2009/2010 El Niño, and were mixed for the 2015/2016 El Niño. Although statistically significant, the magnitudes of the dry-season anomalies were not substantial. Our findings provide additional evidence that photosynthesis of moist tropical Amazon forest increases during the dry season and narrows the potential drivers of perturbations to the atmospheric CO₂ growth rate during the last four ENSO events, as anomalies in dry-season greenness, SIF, and photosynthesis during these ENSO events were minute.

1. Introduction

The seasonal dynamics of forest canopy structure and function in the Amazon are critically important to the local, regional, and global carbon and water cycles, but the dynamics of photosynthesis in moist tropical Amazon forest have been the subject of intense debates over the last two decades (Doughty et al., 2019; Galvão et al., 2011; Huete et al., 2006; Lee et al., 2013; Morton et al., 2014; Saleska et al., 2016; Saleska et al.,

2007; Samanta et al., 2010; Xiao et al., 2006; Xiao et al., 2005). A limited number of field studies at the leaf and canopy (Albert et al., 2018; Wu et al., 2018) and landscape (Restrepo-Coupe et al., 2013; Saleska et al., 2003) levels have assessed the seasonal dynamics of forest canopy structure and function, and have concluded that canopy photosynthetic capacity (greenness) and photosynthesis, or gross primary production (GPP), increased during in the dry season. Several satellite-based studies have concluded that dry-season increases in canopy greenness remained

* Corresponding author at: Department of Microbiology and Plant Biology, University of Oklahoma, 101 David L. Boren Blvd., Norman, OK 73019-5300, USA.
E-mail address: xiangming.xiao@ou.edu (X. Xiao).

<https://doi.org/10.1016/j.rse.2020.112196>

Received 31 March 2020; Received in revised form 10 November 2020; Accepted 13 November 2020

0034-4257/© 2020 Elsevier Inc. All rights reserved.

after adjusting surface reflectance data to account for the effect of viewing and illumination geometry on vegetation indices (Guan et al., 2015; Maeda et al., 2014; Saleska et al., 2016). A recent field study provided *in situ* video evidence of forest canopy dynamics of mixed age leaves and new leaf flush during the dry season (Gonçalves et al., 2020). In our previous study, we documented significant dry-season increases in solar-induced chlorophyll fluorescence (SIF), which is a small amount of energy emitted by plants after chlorophyll absorbs photosynthetically active radiation (PAR), that could not be explained alone by changes in sun-sensor geometry, cloud cover, or sunlight entering the canopy (Doughty et al., 2019).

It has also been debated whether severe meteorological drought associated with El Niño further increases dry-season photosynthesis of moist tropical forests in the Amazon or suppresses it (Asner and Alencar, 2010; Brando et al., 2010; Gatti et al., 2014; Huete et al., 2006; Liu et al., 2017; Samanta et al., 2010; Xu et al., 2011). The atmospheric CO₂ growth rate was historically high during the 2015/2016 El Niño (Betts et al., 2016), and two studies partially attributed the high rate to a large reduction in photosynthesis of tropical South America (Gloor et al., 2018; Liu et al., 2017). Another study reported seemingly conflicting results in that GOME-2 SIF decreased but greenness increased during the 2015/2016 El Niño (Yang et al., 2018b), and another study found that the 2015/2016 El Niño suppressed SIF after a multi-step correction of the GOME-2A data (Koren et al., 2018), which suffers from sensor degradation (Zhang et al., 2018).

Our limited understanding on the effects of ENSO events on moist tropical forests not only have significant implications for dynamic global vegetation models (DGVMs), some of which have poorly represented the seasonal dynamics of photosynthesis in the Amazon (Restrepo-Coupe et al., 2017), but also have important implications for identifying the factors that drive changes in net carbon fluxes as estimated by atmospheric inversions. The net carbon fluxes in the Amazon is the difference between photosynthesis and respiration. Thus, we must discern what drives changes in photosynthesis in the Amazon to understand to what degree and why net carbon exchange has changed and how it may change in the future. Satellite-based observations and data are the only resources that allow us to investigate the Amazon at the basin scale to assess whether what we observe *in situ* at experimental sites is occurring in other parts of the basin.

Here, we used monthly MODIS-based vegetation indices, SIF data from GOME-2 and OCO-2, and photosynthesis estimates from the Vegetation Photosynthesis Model (GPP_{VPM}) for 2007–2017 to investigate (1) if there were dry-season increases in greenness, SIF, and photosynthesis for moist tropical forests, and (2) whether dry-season greenness, SIF, and photosynthesis during the strong El Niños (2009/2010 and 2015/2016) and La Niñas (2007/2008 and 2010/2011) were anomalously high or low for moist tropical forest and the entire Amazon Basin.

We hypothesized that (1) greenness, SIF, and photosynthesis of moist tropical forests increase during the dry season, and (2) dry-season greenness, SIF, and photosynthesis were higher than normal during the El Niños and lower than normal during the La Niñas. We expected these two El Niños to enhance dry-season greenness, SIF, and photosynthesis in moist tropical forest (>2000 mm mean annual precipitation) because these forests are generally radiation limited rather than water limited (Guan et al., 2015) and these two El Niños were preceded by relatively normal amounts of wet season precipitation (Fig. 1), and thus increased radiation should increase greenness, SIF, and photosynthesis (Saleska et al., 2007; Wagner et al., 2017). Conversely, we expected dry-season greenness, SIF, and photosynthesis to be anomalously low during the 2007/2008 and 2010/2011 La Niñas due to the anomalously low amounts of precipitation preceding the dry season of both La Niñas (Fig. 1).

2. Methods

2.1. Study sites

We investigated changes in satellite-based vegetation indices, SIF, and photosynthesis at the K34 eddy flux tower site (2.61°S, 60.21°W), which was part of the Large-Scale Biosphere Atmosphere Experiment in Amazonia (LBA) (Keller et al., 2004), and the Amazon Tall Tower Observatory (ATTO) site (2.15°S, 59.0°W) (Fig. S1) (Andreae et al., 2015), both of which were in the State of Amazonas, Brazil. We also investigated the changes in satellite-based vegetation indices, SIF, and photosynthesis for (1) moist tropical forests and (2) all vegetation types in the basin. Unless otherwise noted, we carried out data analysis at the spatial resolutions of 0.5° and 1.0° (latitude and longitude) to match the spatial

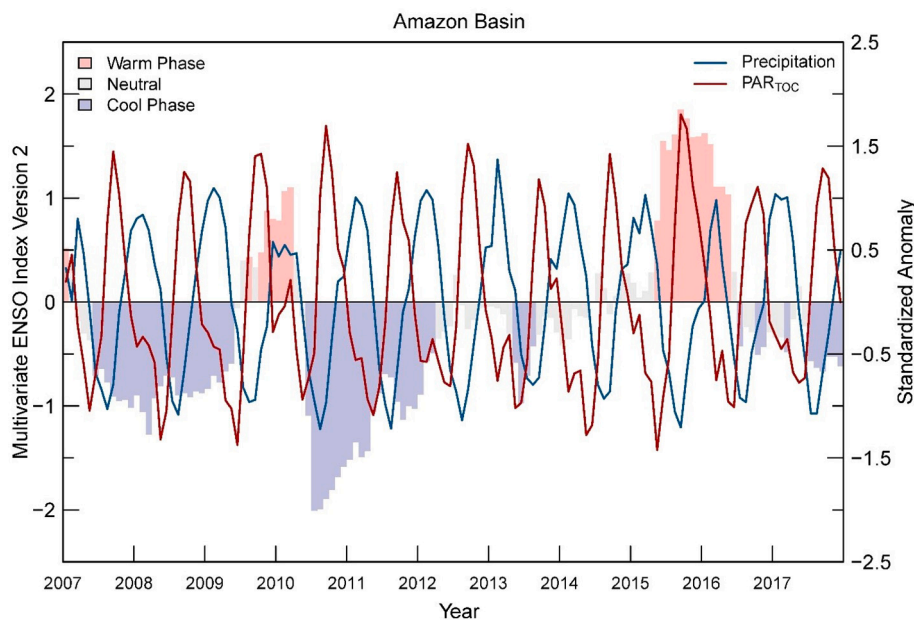


Fig. 1. Monthly Multivariate ENSO Index Version 2 and standardized anomaly of precipitation and photosynthetically active radiation at the top of the canopy (PAR_{TOC}) for the Amazon Basin in 2007 through 2017.

resolutions of GOME-2 and OCO-2 SIF data, respectively. The geographic coordinates for these sites, the percentage of forest cover in their respective 0.5° and 1.0° gridcells, and the percentage of forest change during the study period is detailed in Table S1.

2.2. Vegetation indices

The Normalized Difference Vegetation Index (NDVI) and Enhanced Vegetation Index (EVI) (Huete et al., 2002) were obtained from the MODIS MOD13C2 V006 monthly data product (Didan, 2015), which had a spatial resolution of 0.05°. Prior to aggregating NDVI and EVI to 0.5°, we removed all poor and marginal quality grid cells using the quality reliability flag (0 = good quality). We further filtered NDVI and EVI by using a minimum threshold of 0.6 and 0.3, respectively. Land Surface Water Index (LSWI) (Xiao et al., 2002) was calculated using the MOD09A1 V006 500 m 8-day land surface reflectance product (Verote, 2015). LSWI, which is also termed normalized difference water index (NDWI) in previous studies, is calculated from the NIR and SWIR bands and is sensitive to water content in the vegetation canopy and soils (Gao, 1996; Xiao et al., 2006; Xiao et al., 2005). Missing LSWI values in the time series data were gap-filled (Zhang et al., 2017). We aggregated MOD09A1-based LSWI data to 0.5-degree spatial resolution.

Previous studies have suggested that the bidirectional reflectance effect caused by sun-sensor geometry was the source of seasonality in MODIS-derived NDVI and EVI (Morton et al., 2014), and that surface reflectance data that is not adjusted with the bidirectional reflectance distribution function (BRDF) is questionable (Hilker et al., 2015). However, several studies have shown that there is a dry-season increase in EVI and NDVI regardless of the MODIS surface reflectance products used, including MOD09, MOD13, MCD43, and Multi-Angle Implementation of Atmospheric Correction (MAIAC), although the frequency of good-quality data and the seasonal magnitudes of change vary among these products (Guan et al., 2015; Hilker et al., 2015; Maeda et al., 2016; Maeda et al., 2014; Saleska et al., 2016). Nevertheless, we incorporated BRDF-adjusted MAIAC (MCD19A1.006) EVI (EVI_{In}) and NDVI (NDVI_{In}) into our analysis. The BRDF-adjusted vegetation indices, EVI_{In} and NDVI_{In}, were provided as an 8-day, 0.05-degree product with global coverage in the Climate Model Grid (CMG) format and was accessed at <https://portal.nccs.nasa.gov/datashare/maiac/DataRelease/>.

For Fig. 2, we aggregated the MAIAC data to 0.5-degree spatial resolution to match the spatial resolution of the other datasets used in the figure; 8-day values are shown. For Fig. 3, we aggregated the MAIAC data to monthly values at 0.5-degree spatial resolution for consistency with the other datasets. For Figs. 4-7 and all statistical analysis, we used the MAIAC data as provided in its original spatial and temporal resolution.

2.3. Solar-induced chlorophyll fluorescence

We used SIF retrievals from GOME-2 and OCO-2, which were available for 2007–2017 and September 2014 – October 2017, respectively. All SIF data analyses were conducted using the data as provided, without removing outliers or negative values. Intra-annual changes in GOME-2 and OCO-2 SIF datasets have been shown to be significantly correlated with eddy flux tower GPP and gridded GPP datasets (Li et al., 2018; Sun et al., 2018; Zhang et al., 2018; Zhang et al., 2016). We used daily average SIF values (SIF_{daily}) provided in the Level 3 (monthly) GOME-2 SIF v27 product from the MetOp-A satellite (Joiner et al., 2013; Joiner et al., 2016) because SIF_{daily} has been shown to have a more consistent relationship with daily GPP than instantaneous SIF (SIF_{inst}) (Zhang et al., 2018c). The GOME-2 SIF products are noisy due to sensor degradation and the inherently low-energy signal of SIF (Joiner et al., 2013). The sensor onboard GOME-2's MetOp-A satellite has degraded at an average of 1.1% a year, thus it is not advisable to conduct long-term trend analyses (Zhang et al., 2018). The sensor degradation causes a decrease in SIF values over time, so this caveat must be considered when interpreting results derived from GOME-2 data. An official data product

that accounts for and corrects the data for sensor degradation has not been released. The coarse spatial resolution of the GOME-2 data inevitably introduces cloud contamination, but the data was filtered to retain only data with effective cloud fractions of <30%.

The OCO-2 v8 SIF Lite data product (B8100) was provided in daily files (Frankenberg et al., 2014). Each file provided SIF retrievals at 757 nm (SIF₇₅₇) and 771 nm (SIF₇₇₁). We averaged the two bands together by first applying a wavelength correction factor of 1.5 to SIF₇₇₁ (Sun et al., 2018). To match the temporal resolution of the GOME-2 data, we averaged the SIF retrievals for each month. The OCO-2 data was provided pre-filtered to exclude poor quality data (Frankenberg, 2015). GOME-2 and OCO-2 SIF values in our study should not be directly compared due to several differences, including spatial resolution, overpass time, sun-sensor geometry, and the wavelengths used to retrieve SIF. OCO-2 SIF was only used in our site-level analysis because the OCO-2 SIF record was not long enough to investigate differences between ENSO-event years and ENSO-neutral years.

2.4. Vegetation Photosynthesis Model

The Vegetation Photosynthesis Model (VPM) is a light-use efficiency model (LUE) (Xiao et al., 2005; Xiao et al., 2004; Zhang et al., 2017). In this model, the fraction of absorbed photosynthetically active radiation ($fPAR$) by vegetation canopy was partitioned into PAR absorbed by chlorophyll ($fPAR_{chl}$) and non-photosynthetic vegetation ($fPAR_{NPV}$). GPP_{VPM} (g C/m²/day) was a product of $fPAR_{chl}$, PAR , and light-use efficiency (ϵ_g):

$$GPP_{VPM} = PAR \times fPAR_{chl} \times \epsilon_g \quad (1)$$

where $fPAR_{chl}$ was estimated as a function of the Enhanced Vegetation Index (EVI), which was calculated using MODIS MOD09A1 V006 data product (Zhang et al., 2017). Maximum LUE (ϵ_0) is higher for C4 plants than C3 plants (Ehleringer et al., 1997; Epstein et al., 1997), and VPM incorporated global C4 vegetation percentage maps (Zhang et al., 2017). The maximum light-use efficiencies used in the model were 0.035 mol CO₂ mol⁻¹ PAR for C3 plants and 0.0525 mol CO₂ mol⁻¹ PAR for C4 plants. Thus, GPP_{VPM} for each gridcell was calculated using the area fraction and light-use efficiency for C3 and C4 vegetation. ϵ_g is regulated by air temperature and water stress (Haxeltine and Prentice, 1996). To account for these stresses, VPM used temperature (T_{scalar}) and water scalars (W_{scalar}) to downregulate maximum light use efficiency (ϵ_0). Both scalars range from 0 to 1 and were calculated as:

$$T_{scalar} = \frac{(T - T_{max}) \times (T - T_{min})}{(T - T_{max}) \times (T - T_{max}) - (T - T_{opt})^2} \quad (2)$$

$$W_{scalar} = \frac{1 + LSWI}{1 + LSWI_{max}} \quad (3)$$

where T , T_{max} , T_{min} , and T_{opt} are daytime mean, maximum, minimum, and optimum air temperature for photosynthesis, respectively. $LSWI_{max}$ is the maximum LSWI for each pixel each year, and is further detailed by Zhang et al. (2017).

We calculated monthly daily average GPP_{VPM} using the data published by Zhang et al. (2017) and available at <https://doi.pangaea.de/10.1594/PANGAEA.879560> by first determining the monthly total and dividing it by the number of days in that month. In Figs. 4-7, and for the statistical analyses that accompany these figures, we aggregated the original 500-m GPP_{VPM} product to 0.05 degree to match the spatial resolution of the MAIAC data. Previous studies have validated VPM in biomes around the world using data from the eddy flux tower sites (Doughty et al., 2018; Xiao et al., 2005; Xin et al., 2017; Zhang et al., 2017; Zhang et al., 2016) and SIF (Cui et al., 2017; Ma et al., 2018) data.

2.5. Climate data

In Figs. 2 and 3, we used air temperature and photosynthetically active radiation (PAR) data from the National Centers for Environmental Prediction (NCEP) Reanalysis 2 dataset, accessed at <https://www.esrl.noaa.gov/psd/>. These data were downsampled to $0.5^\circ \times 0.5^\circ$ using a non-linear, distance-weighted spatial interpolation technique (Zhang et al., 2017; Zhao et al., 2005). Monthly precipitation data was obtained from the Tropical Rainfall Measuring Mission's (TRMM) Multi-Satellite Precipitation Analysis (TMPA) (Huffman et al., 2007). We aggregated the 3B43 v7 data product (Huffman et al., 2014) to $0.5^\circ \times 0.5^\circ$ from its original spatial resolution of $0.25^\circ \times 0.25^\circ$. ENSO periods were determined using the indices in Fig. 1, as provided by the Multivariate El Niño Southern Oscillation Index Version 2 (MEI.v2) available at <https://www.esrl.noaa.gov/psd/enso/mei/> (Volter and Timlin, 2011). For Fig. 1, we used the monthly ERA5 Reanalysis Dataset (Climate Change Service, 2020). ENSO phases shift in the middle of the calendar year, typically between June and July. Thus, we use a two-year naming convention to describe an ENSO event (e.g. 2010/2011 La Niña).

2.6. Forest cover

To determine changes in forest cover area during the study period (2007–2017), we mapped annual forest cover with a spatial resolution of 500-m using our previously published methods (Qin et al., 2019; Qin

et al., 2016). Only gridcells that were consistently forest and non-forest were used in our study, and moist tropical forest were defined as those pixels that were consistent forest and had a mean annual precipitation (MAP) of more than 2000 mm as calculated using TRMM data for our study period of 2007–2017.

2.7. Statistical analyses

We used one-sample *t*-tests for GOME-2 SIF, GPP, EVIn, and NDVIn (Figs. 4–7) to determine if the difference between normal September or dry-season SIF and September or dry-season SIF during the La Niñas and El Niños was significantly different than zero. Statistical results, including number of gridcells, change, 95% confidence intervals, *t*-values, *p*-values, and percentage change are reported in Tables S2–5.

3. Results

3.1. Dry-season increase of canopy greenness, SIF, and photosynthesis

First, we examined the seasonality of satellite-based greenness, SIF, and photosynthesis at two moist forest sites, the Amazon Tall Tower (ATTO) and the Manaus K34 eddy tower. We estimated the forest cover within each of the 1-degree gridcells at these sites to be 99% and 96%, respectively, and the forest cover decreased relatively little over the 11-year study period (−0.2% and −0.3%; Table S1). In terms of seasonal

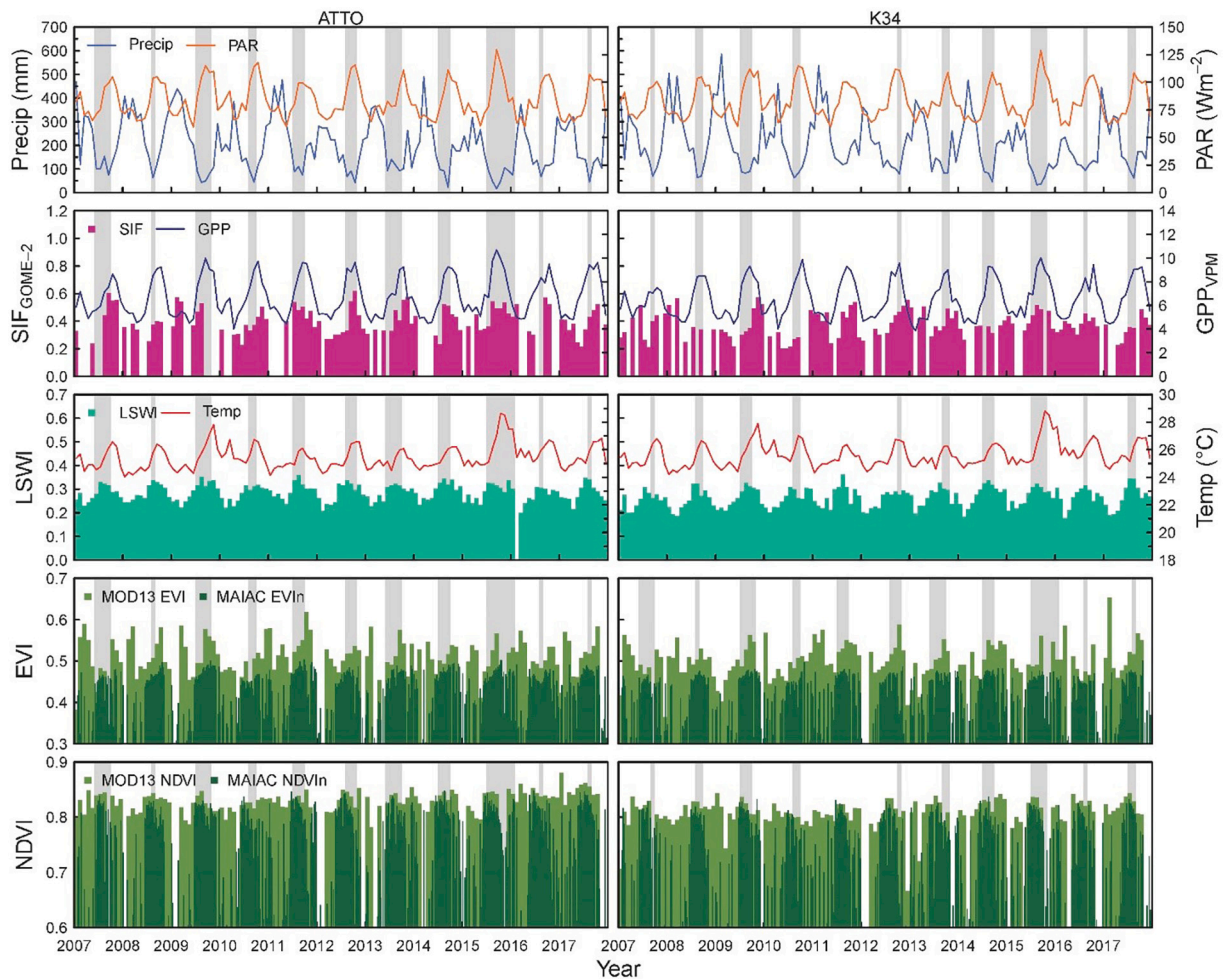


Fig. 2. Monthly dynamics of climate, GOME-2 SIF, GPP_{VPM} , and greenness at the ATTO and K34 sites. Continuous data shown as lines. Shaded areas are months in which monthly total precipitation was less than 100 mm. Shown are monthly total precipitation (mm month^{-1}), photosynthetically active radiation (PAR), solar induced chlorophyll fluorescence (SIF; $\text{mw}^{-2} \text{m}^{-2} \text{nm}^{-1} \text{sr}^{-1}$), gross primary production (GPP; $\text{gC m}^{-2} \text{day}^{-1}$), land surface water index (LSWI), temperature, and enhanced vegetation index (EVI) and normalized vegetation difference index (NDVI) from MODIS and BRDF-adjusted MAIAC (EVIn; NDVIn) products.

dynamics, Enhanced Vegetation Index (EVI) and Land Surface Water Index (LSWI), which respectively provide information on canopy chlorophyll and water content, increased during the dry season and decreased during the wet season (Fig. 1). EVI and LSWI are synchronized because of the seasonal dynamics of new leaf emergence and flush, leaf aging, senescence, and fall. As new leaves flush through the dry season, the canopy chlorophyll and water content increases, and as leaves age in the wet season they lose chlorophyll and water, senesce, and fall to the forest floor in the early dry season. We found that the seasonality of monthly GOME-2 and OCO-2 SIF at both sites also increased during the dry season (Figs. 2, S1), which agreed with our previously reported results using SIF data from the TROPOspheric Monitoring Instrument (TROPOMI) (Doughty et al., 2019). For these two moist forest sites, EVI, LSWI, SIF, and GPP_{VPM} increased during the dry season (July–December) and decreased during the wet season (January–June).

At the basin scale, we found that GOME-2 SIF and photosynthesis were most often higher during September (typically the driest month) than during March (typically the wettest month) for those gridcells that had $\geq 80\%$ forest cover and ≥ 2000 mm mean annual precipitation (Fig. S2). For those gridcells that had $<80\%$ forest cover, SIF and photosynthesis were often higher in March. This phenomenon was also observed by a previous analysis that found that increases in dry-season EVI and SIF for tropical forests was largely determined by whether the forest had a mean annual precipitation (MAP) threshold of 2000 mm a year (Guan et al., 2015).

3.2. Anomalies of dry-season greenness, SIF, and photosynthesis during La Niña and El Niño at two moist tropical forest sites

As illustrated in Fig. 3, monthly dry-season greenness, GOME-2 SIF, and GPP_{VPM} during the 2009/2010 El Niño and 2015/2016 El Niño

events were often higher than the multi-year mean and the preceding La Niña events at ATTO and K34. Note that some gaps appear in the data due to cloud cover and poor-quality observations. The air temperature and precipitation panels in Fig. 3 indicate that these higher mean values of greenness, SIF, and photosynthesis during El Niños coincided with lower mean precipitation, and higher than normal air temperature, LSWI, and PAR. Thus, our results indicate (1) that these two sites did not become water limited during the two El Niño dry-seasons, and (2) that higher dry-season SIF and GPP_{VPM} during the El Niños were likely driven by a combination of higher PAR, canopy chlorophyll content (EVI), and canopy water content (LSWI).

3.3. Anomalies of dry-season greenness, SIF, and GPP_{VPM} during La Niña and El Niño for moist tropical forest and the Amazon Basin

We further investigated anomalies of September and dry-season greenness, GOME-2 SIF, and GPP_{VPM} during the two El Niños and La Niñas. We found that September SIF, GPP, EVI, and NDVI during the 2009/2010 El Niño were significantly higher than normal, and significantly lower than normal during the preceding La Niñas of 2007/2008 for both the entire basin and moist tropical forests (Fig. 4; Table S2). At the basin scale, September SIF, GPP, EVI, and NDVI were about 12%, 4.1%, 2.8%, and 1.9% higher than normal during the 2009/2010 El Niño, and were about 11%, 3.7%, 3.9%, and 1.9% lower than normal during the 2007/2008 La Niña, respectively. For moist tropical forests, September SIF, GPP, EVI, and NDVI were about 8.8%, 5.8%, 1.9%, and 0.7% higher than normal during the 2009/2010 El Niño, and were about 6.7%, 6.3%, 3.9%, and 1.5% lower than normal during the 2007/2008 La Niña, respectively.

For the 2010/2011 La Niña and 2015/2016 El Niño, September GOME-2 SIF, GPP_{VPM} , EVI, and NDVI were significantly higher during

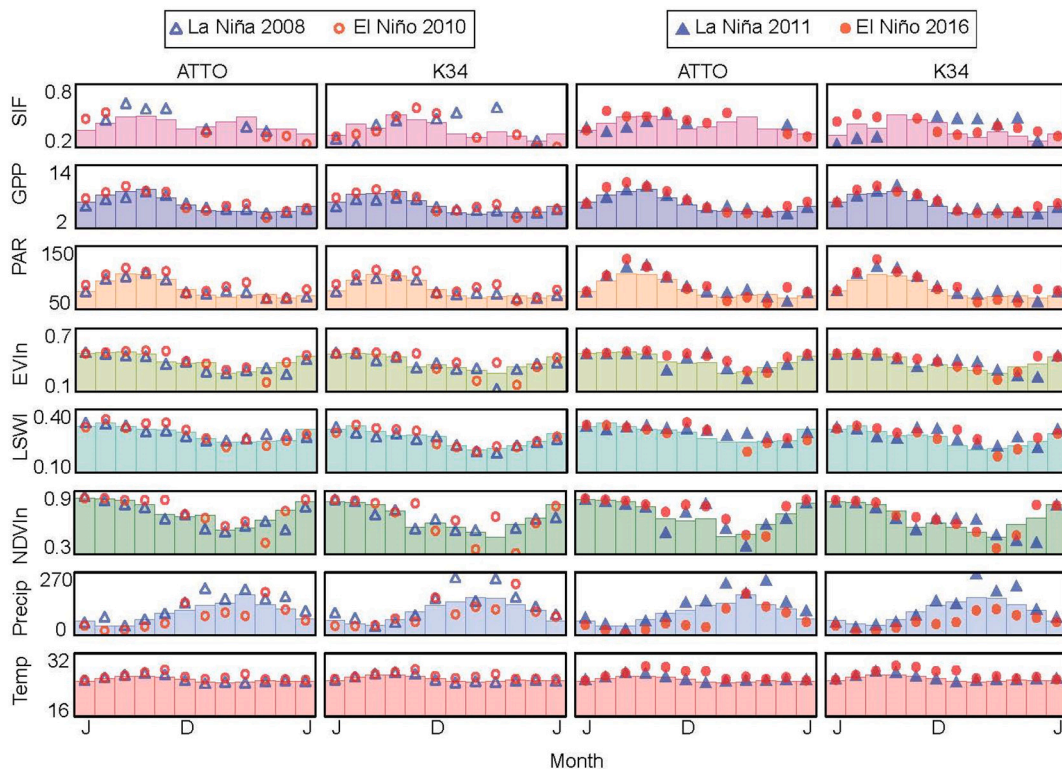


Fig. 3. ENSO year (July – June) seasonal dynamics of monthly mean GOME-2 SIF, photosynthesis, greenness, and climate at ATTO and K34. Symbols are monthly observations during La Niña (blue triangles) and El Niño (red circles) and bars are monthly means from 2007 to 2017 (excluding the La Niña and El Niño events). The left two panels show the 2007/2008 La Niña and 2009/2010 El Niño. The right two panels show the 2010/2011 La Niña and 2015/2016 El Niño. Illustrated are monthly mean SIF ($\text{mw}^{-2} \text{m}^{-2} \text{nm}^{-1} \text{sr}^{-1}$), GPP is GPP_{VPM} ($\text{gC m}^{-2} \text{day}^{-1}$), PAR (Wm^{-2}), EVI, LSWI, NDVI, total monthly precipitation (mm month^{-1}), and temperature ($^{\circ}\text{C}$). (For interpretation of the references to colour in this figure legend, the reader is referred to the web version of this article.)

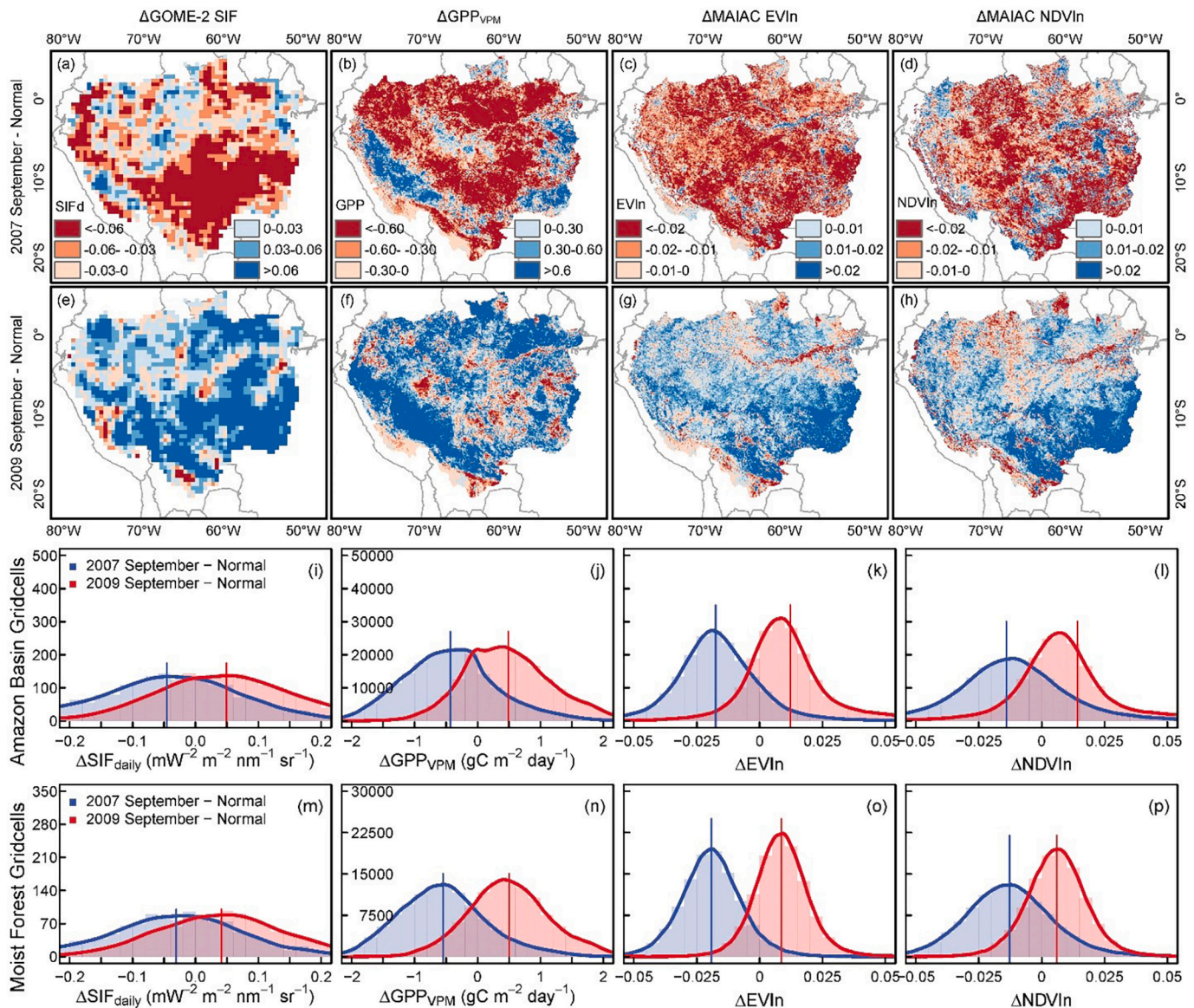


Fig. 4. Anomalies of September GOME-2 SIF, GPP_{VPM} , EVIn, and NDVI in the Amazon. Anomalies were calculated as the La Niña or El Niño September minus the mean of the normal years, thus negative values indicate lower than normal and positive values indicate higher than normal. Frequency histograms in each column (i-p) correspond to the maps (a-h) above them. We used a one-sample *t*-test at the 95% level of confidence to test if the differences were significantly different from zero (Table S2). Moist forest gridcells were those with >80% forest cover and > 2000 mm mean annual precipitation.

the El Niño than the La Niña that preceded for both the Amazon Basin and moist tropical forests (Fig. 5; Table S3). At the basin scale, September SIF, GPP_{VPM} , EVIn, and NDVI were significantly lower than normal during the La Niña and significantly higher than normal during the El Niño. Results were similar for the moist tropical forests, except that September GPP_{VPM} was significantly higher than normal during the La Niña and EVIn was significantly lower than normal during the El Niño.

As for the dry season, the anomalies of GOME-2 SIF, GPP_{VPM} , EVIn, and NDVI during the ENSO events were much more subtle than the September anomalies, although significant. At the basin scale, dry-season SIF, GPP_{VPM} , EVIn, and NDVI were about 6.7%, 2.8%, 1.1%, and 0.8% higher than normal during the 2009/2010 El Niño, and were about 0.5%, 3.4%, 2.5%, and 0.8% lower than normal during the 2007/2008 La Niña (Fig. 6; Table S4). Results for these two ENSO events were similar for moist tropical forests except for dry-season SIF during the 2007/2008 La Niña, which was 0.7% higher than normal. However, SIF

values from the early years of the GOME-2 mission are relatively higher than during the later years because there was little to no sensor degradation.

Our results were inconsistent or inconclusive on whether dry-season GOME-2 SIF, GPP_{VPM} , EVIn, or NDVI were higher or lower than normal, particularly for the 2015/2016 El Niño because of GOME-2 sensor degradation in the later years of the GOME-2 mission. Dry-season SIF, GPP_{VPM} , EVIn, and NDVI at the basin scale during the 2010/2011 La Niña were significantly slightly lower than normal by about 2.3%, 0.1%, 2.5%, and 1.9%, respectively (Fig. 7; Table S5). The moist tropical forests had similar lower than normal values, except for GPP which was marginally higher than normal by <0.1%. Dry-season results were split for the 2015/2016 El Niño at the basin scale and for moist forest, with significantly lower than normal SIF (3.6% and 4.4%) and EVIn (0.5% and 0.8%) and significantly higher than normal GPP_{VPM} (2.2% and 2.7%) and NDVI (0.3% and 0.1%). For the negative SIF anomaly during the 2015/2016 El Niño, the apparently lower than

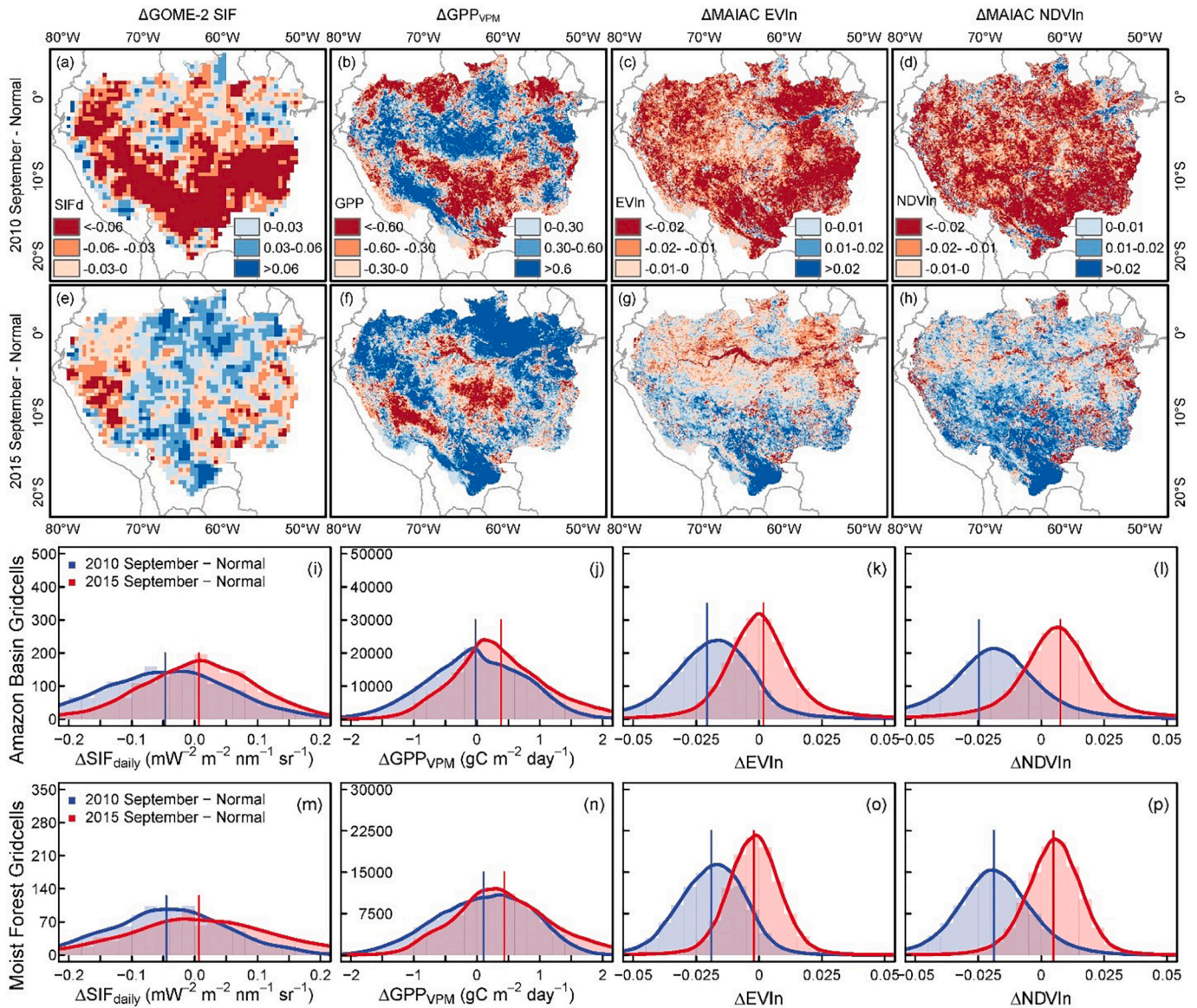


Fig. 5. Anomalies of September GOME-2 SIF, GPP_{VPM} , EVIn, and NDVIIn during the 2010/2011 La Niña and 2015/2016 El Niño in the Amazon. Anomalies were calculated as the La Niña or El Niño September minus the mean of the normal years, thus negative values indicate lower than normal and positive values indicate higher than normal. Frequency histograms in each column (i-p) correspond to the maps (a-h) above them. We used a one-sample t-test at the 95% level of confidence to test if the differences were significantly different from zero (Table S3). Moist forest gridcells were those with >80% forest cover and >2000 mm mean annual precipitation.

normal values are largely driven by GOME-2 sensor degradation (Zhang et al., 2018), so the negative anomaly is not as severe as it appears, or could possibly be positive.

4. Discussion

4.1. Dry-season increases of greenness, SIF, and GPP

Our findings on the dry-season increase of greenness, SIF, and GPP_{VPM} for the two forest sites in the Amazon agree with the results reported for the LBA eddy flux towers (Restrepo-Coupe et al., 2013), *in situ* observations of leaf flush, litterfall, and photosynthesis (Doughty et al., 2015; Rice et al., 2004; Saleska et al., 2003), prior satellite observations (Doughty et al., 2019; Huete et al., 2006; Saleska et al., 2007; Xiao et al., 2005), and more recent *in situ* studies that observed greening and leaf flush using tower-based cameras (Gonçalves et al., 2020; Lopes et al., 2016; Wu et al., 2016). Importantly, the Vegetation

Photosynthesis Model (VPM) was able to capture well the observed seasonality of photosynthesis, which has been poorly captured by several DGVMs that have simulated dry-season declines in GPP (Restrepo-Coupe et al., 2017).

The dry-season increase in greenness, SIF, and GPP can be explained by the shedding of lianas and old leaves (4 to 5 years old) in the forest canopy, the exposure of mid-age and young leaves, and new leaf flush (Brando et al., 2010; Gonçalves et al., 2020; Xiao et al., 2005). The amount of litterfall during the dry seasons are more than compensated for by new leaf production (Wu et al., 2016). In addition, bud development is queued by the length of day (Rivera et al., 2002), but leaf flushing and development coincides with increased radiation (Wright and Van Schaik, 1994) and water availability (Brando et al., 2010).

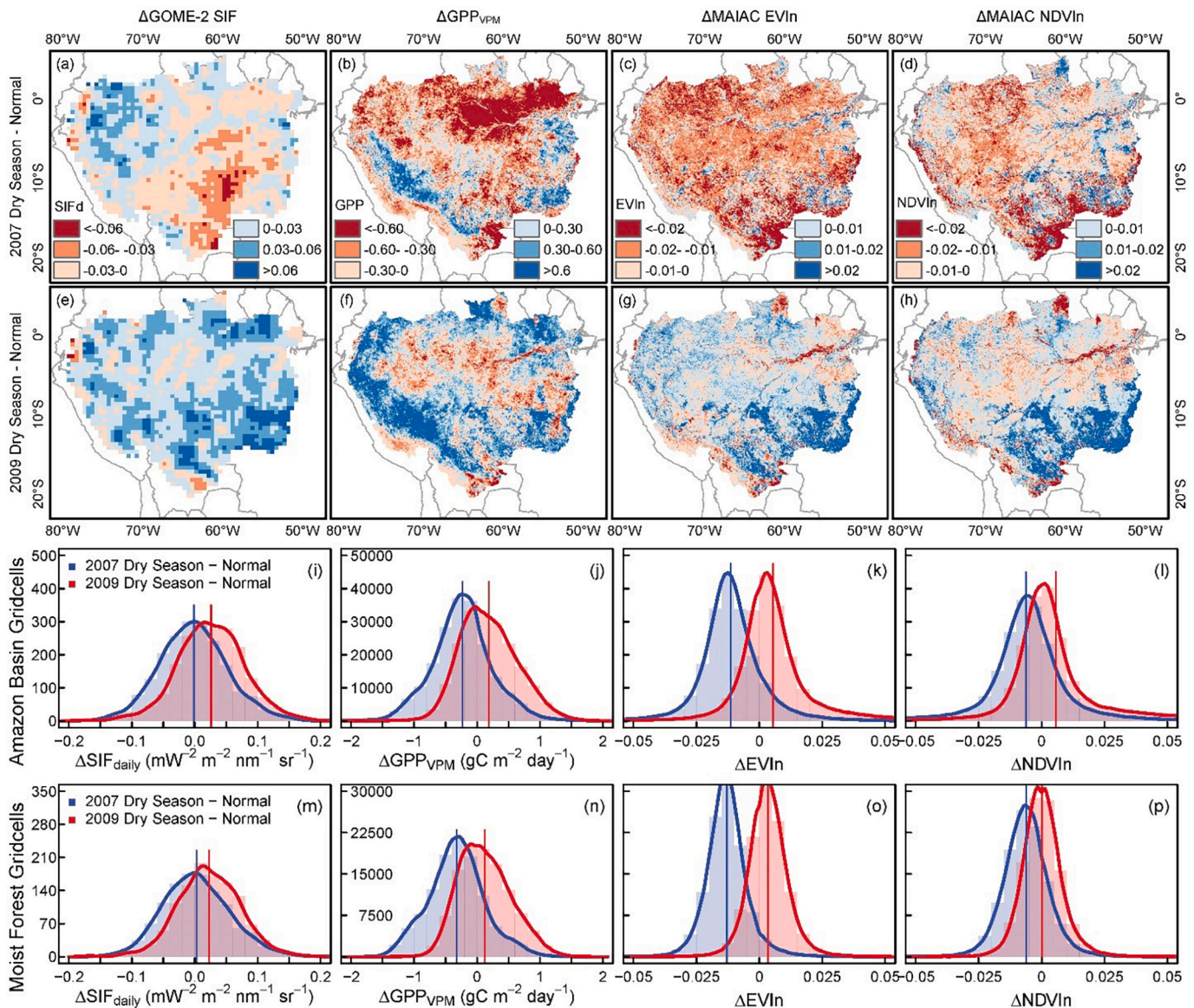


Fig. 6. Anomalies of dry-season GOME-2 SIF, GPP_{VPM} , EVIn, and NDVI in the Amazon. Anomalies were calculated as the La Niña or El Niño dry-season (Jun-Oct) minus the mean of the normal years, thus negative values indicate lower than normal and positive values indicate higher than normal. Frequency histograms in each column (i-p) correspond to the maps (a-h) above them. We used a one-sample t-test at the 95% level of confidence to test if the differences were significantly different from zero (Table S4). Moist forest gridcells were those with >80% forest cover and >2000 mm mean annual precipitation.

4.2. Anomalies of dry-season greenness, SIF, and GPP during El Niño and La Niña

For moist Amazon forests with relatively little water limitation due to high mean annual precipitation (>2000 mm) and deep root systems (Nepstad et al., 1994), it is plausible that leaf flush and bud development occur quicker and/or sooner in drier years when PAR increases sooner and is higher due to less frequent and/or less dense cloud cover than normal (Brando et al., 2010; Saleska et al., 2007; Wagner et al., 2017). These physiological responses of the moist tropical forest to changes in solar illumination and the lack of anomalously low precipitation preceding the dry season can explain why we observed positive anomalies in dry-season greenness, SIF, and GPP_{VPM} at both the site level and basin scale during the 2009/2010 and 2015/2016 El Niños. However, the negative anomalies in dry-season greenness, SIF, and GPP_{VPM} for moist forest during the La Niñas indicates that dry seasons preceded by anomalously low precipitation may indeed impact the dry-season

productivity of moist forest, in addition to low dry-season precipitation as was seen during the 2010/2011 La Niña dry season (Lewis et al., 2011).

We found that the September anomalies in greenness, SIF, and GPP_{VPM} during the ENSO events were substantially larger than the dry-season anomalies, which suggested that there was likely a shift in leaf demography and the timing of leaf flushing in these years. Phenocam data from Amazon tower sites has shown that these shifts can be driven by environmental conditions and can be captured by satellite remote sensing (Gonçalves et al., 2020). For the moist forest, it is possible that leaf flush occurred sooner during the two El Niños and occurred later during the La Niñas, resulting in much larger anomalies in greenness, SIF, and GPP_{VPM} in September than the entire dry season. In any case, our results concur with previous studies which highlight that canopy dynamics, leaf demography, and phenology are important determinants of intra- and interannual changes in greenness and GPP rather than changes in cloud cover and incoming solar radiation alone (Gonçalves

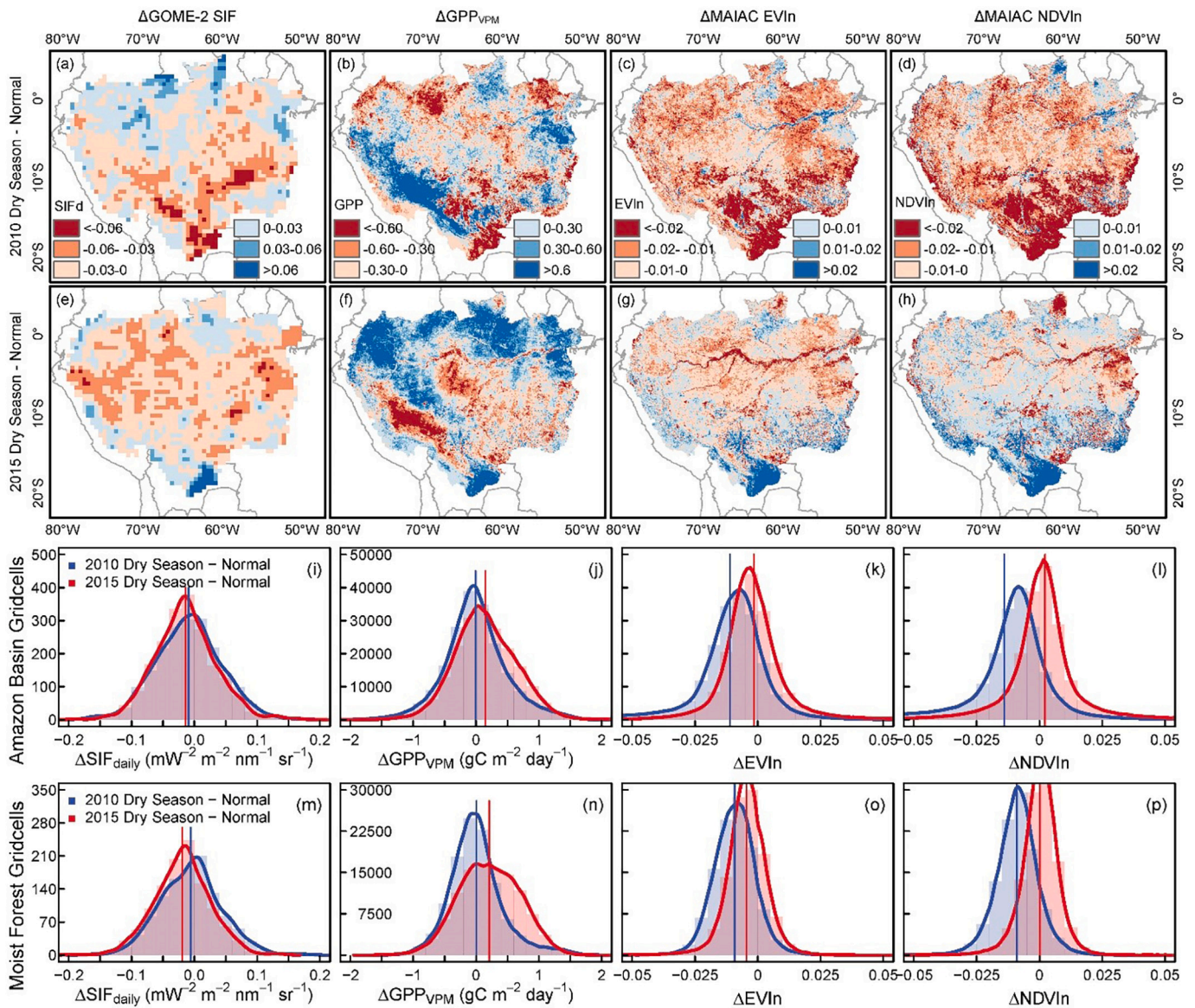


Fig. 7. Anomalies of dry-season GOME-2 SIF, GPP_{VPM} , EVIn, and NDVI in the Amazon. Anomalies were calculated as the La Niña or El Niño dry-season (Jun-Oct) minus the mean of the normal years, thus negative values indicate lower than normal and positive values indicate higher than normal. Frequency histograms in each column (i-p) correspond to the maps (a-h) above them. We used a one-sample t-test at the 95% level of confidence to test if the differences were significantly different from zero (Table S5). Moist forest gridcells were those with >80% forest cover and >2000 mm mean annual precipitation.

et al., 2020; Wagner et al., 2017; Wu et al., 2016).

Like the September anomalies during the El Niños and their preceding La Niñas, dry-season greenness, SIF, and GPP_{VPM} was also higher during the El Niños than their preceding La Niñas except for SIF during the 2015/2016 El Niño. However, it cannot be concluded that GOME-2 SIF was truly lower than normal during the 2015/2016 El Niño because of GOME-2 sensor degradation (Zhang et al., 2018).

The anomalies of greenness, SIF, and GPP_{VPM} at the basin scale and for moist tropical forest were similar not only because the moist tropical forest comprises a large proportion of the basin, but it could also be due to similar drought responses by moist tropical and seasonally moist forests (Barros et al., 2019). The seasonal cycle of SIF is similar for forest and non-forest in the Amazon because crops are typically harvested around midyear and replanted during the latter half of the year (Dougherty et al., 2019). Thus, anomalously low precipitation prior to planting may explain the relatively larger negative anomalies in greenness, SIF, and GPP_{VPM} in the southern region of the Amazon where

croplands and pastures are concentrated (Fig. 7).

4.3. Meteorological drought and ENSO events

Meteorological drought severity is temporally and spatially heterogeneous within and across drought events (Lewis et al., 2011; Marengo et al., 2008), making each drought even unique. The effect of meteorological drought during the dry season on the Amazonian carbon cycle is complex because the moist tropical forest experiences less cloud cover and increased sunlight and air temperature during a period when water availability and air temperature may not limit photosynthesis (Brandt et al., 2010; Condit et al., 2004; Graham et al., 2003). Higher air temperatures and drought are suspected to increase ecosystem respiration and tree mortality, which may offset any potential increases in photosynthesis and result in a decline in the net carbon sink (Hubau et al., 2020). Furthermore, the legacy effects of drought on tree mortality (Dougherty et al., 2015; Nepstad et al., 2007; Phillips et al., 2009), fire

frequency and severity (Aragao et al., 2008, Aragao et al., 2007), phenology (Gonçalves et al., 2020), and canopy structure (Saatchi et al., 2013) may linger long after drought and can have positive feedbacks (Laurance and Williamson, 2001). Thus, the impacts of drought at the landscape scale is a mosaic of localized, immediate, and long-term responses driven by site-specific characteristics, history, and climate rather than a homogeneous response.

Likewise, ENSO events are unique because they differ in space, time, and amplitude, and their teleconnections can differ (Capotondi et al., 2015). For instance, the 2010 Amazon drought (Lewis et al., 2011) event mostly affected the western and southern Amazon Basin and was driven by an El Niño and North Atlantic warming (Marengo et al., 2011), whereas the 2015/2016 ENSO-driven drought was unprecedented and largely affected the northern and southeastern regions (Jiménez-Muñoz et al., 2016). Our findings that anomalies in dry-season greenness, SIF, and GPP_{VPM} were generally negative during the two La Niñas and generally positive during the El Niños should not be misinterpreted as responses that are characteristic of either ENSO event. Rather, it is more likely that dry-season photosynthesis in the Amazon is determined in part by the amount of precipitation preceding the dry season and the amount of PAR reaching the canopy during the dry season, irrespective of the ENSO phase.

4.4. Atmospheric carbon dioxide, the 2015/2016 El Niño, and the Amazon

Anomalous increases in the rate of growth of atmospheric CO₂ during El Niños has been noted for several decades (Bacastow, 1976; Keeling et al., 1995; Keeling and Revelle, 1985). Newly launched satellites that provide estimates of atmospheric CO₂ and SIF, such as GOME-2, OCO-2/3, and TROPOMI, open new opportunities to investigate and better understand the relationship between anomalous increases in the atmospheric CO₂ growth rate and changes in photosynthesis during El Niños. The 2015/2016 El Niño was one of the strongest ENSO events on record (Santoso et al., 2017), contributed to the highest annual growth rate in atmospheric CO₂ on record (Betts et al., 2016), and occurred shortly after the launch of OCO-2, making this ENSO event of particular interest to the scientific community.

Our results indicated that the large increase in atmospheric CO₂ during the 2015/2016 El Niño was not contributed to by a large decrease in dry-season photosynthesis in the Amazon. Thus, if there was a reduction in tropical South American photosynthesis during this El Niño, the reduction must have occurred outside of the dry season and/or outside of the Amazon Basin. A recent study did attribute an anomalously large release of carbon from the Amazon during the 2015/2016 El Niño to decreased photosynthesis as diagnosed by SIF during October 2015 to March 2016, which is a period of time that largely falls outside of our definition of dry season (Gloor et al., 2018). Although fires increase atmospheric CO₂, this same study found fires in the Amazon had only a minor contribution to the increase in the atmospheric CO₂ growth rate.

We also found that although there were statistically significant anomalies in dry-season greenness, GOME-2 SIF, and GPP_{VPM} during the two El Niños and La Niñas, their magnitudes were not large. Our findings are particularly important for understanding changes in dry-season greenness, SIF, and photosynthesis during the last two La Niñas, which have received very little attention in previous studies due to a nearly exclusive focus on El Niño. Future research into dry-season greenness, SIF, and photosynthesis should consider the environmental conditions and ENSO phase preceding the dry-season, because the dry season begins at roughly the same time as ENSO phases shift in June and July. Thus, it could be the case that the amount of precipitation preceding a dry season asserts a greater influence on the dry-season greenness, SIF, and photosynthesis than the phase preceding or occurring during the dry season itself.

4.5. Potential impact of cloud cover on our results and spaceborne SIF retrievals

Spaceborne-retrieved SIF is sensitive to changes in canopy physiology and phenology, but these SIF retrievals can also be affected by cloud cover due to its ability to shield or diffuse SIF away from the spaceborne sensor. This effect of cloud cover on SIF retrievals does force the question of whether reduced cloud cover during El Niño explains the increase in GOME-2 SIF, and likewise whether increased cloud cover during La Niña decreased GOME-2 SIF. This question is fair, particularly given that GOME-2 has a relatively coarse resolution and cloudless scenes of the Amazon would be rare, although the data was filtered to include only retrievals with <30% cloud cover. To address this question, we will first discuss the spatial and temporal consistency between the anomalies of greenness, SIF, and GPP_{VPM} we reported. Then, we discuss some important caveats that are specific to the impact of cloud cover on spaceborne SIF retrievals.

We preface this discussion by pointing out that cloud cover anomalies during each ENSO event can vary widely, and a recent study found no widespread anomalies in Amazon cloud cover during the two El Niños in our study (Jimenez et al., 2018), but comparable studies on cloud cover during La Niña are lacking. However, we did note that dry-season photosynthetically active radiation at the top of the canopy (PAR_{TOC}) during the 2010/2011 La Niña and the 2015/2016 El Niño were extremely similar, yet there were different responses in dry-season greenness, SIF, and GPP_{VPM} (Fig. 1). Also, in our previous study we highlighted that high resolution spaceborne SIF data from the TROPospheric Monitoring Instrument (TROPOMI) and eddy tower GPP data showed increased SIF and GPP in the moist forest for several weeks in the late dry season as PAR_{TOC} decreased and cloud cover increased (Doughty et al., 2019). Thus, *in situ* measurements and spaceborne SIF retrievals indicate that our observed changes in greenness, SIF, and GPP_{VPM} were strongly driven by canopy dynamics rather than solar irradiance alone.

The anomaly maps of GOME-2 SIF in the first two rows of Figs. 4-7 show high spatial consistency with GPP_{VPM}, EVIn, and NDVIn. The vegetation indices that feed the VPM model, EVI and LSWI from MOD09, and the BRDF-adjusted EVIn and NDVIn from MAIAC used in our comparison were rigorously filtered for clouds and quality. Thus, the spatial agreement between GOME-2 anomalies and anomalies of GPP_{VPM}, EVIn, and NDVIn for each La Niña and El Niño suggest that cloud cover is not the sole driver of the GOME-2 anomalies we have presented, but rather cloud cover may partially explain inconsistencies between the GOME-2 anomalies and the GPP_{VPM}, EVIn, and NDVIn anomalies.

There are some important caveats when considering the impact of cloud cover on spaceborne SIF retrievals. First, the effect cloud cover on retrieved SIF at a given point in time is the product of two factors: (1) the percentage of a satellite sounding footprint that contains clouds and (2) cloud thickness. The cloud area fraction for each GOME-2 footprint can be determined and was used as a quality control filter of the data, but cloud thickness and its homogeneity cannot be ascertained. Although investigations into cloud frequency and percentage area cover may provide some anecdotal evidence of what might drive intra or interannual changes in SIF, the findings from such an inquiry would be met with some degree of skepticism and uncertainty given that cloud optical thickness cannot be determined. For instance, under the exact same environmental, illumination, and vegetation conditions, two gridcells with 30% cloud cover may yield very different SIF retrievals because of differences in cloud optical thickness. However, SIF is substantially less affected by cloud optical thickness than vegetation indices and the surface reflectance from which they are derived (Guanter et al., 2015). Thus, this relatively weak impact of cloud cover on spaceborne SIF retrievals may explain why there is a strong spatial agreement between the anomalies of GOME-2 SIF and vegetation indices, which were filtered for clouds and quality.

Second, although clouds may block or diffuse some of the SIF emission from the satellite sensor, clouds are also shading the canopy and could be reducing SIF and photosynthesis due to reduced PAR. Thus, the decreased SIF signal retrieved from the satellite sensor in this case could be somewhat representative of, although overestimate, a decrease in SIF emission from the canopy, particularly for GOME-2 as its overpass is during the morning before the canopy has become light saturated by midday solar illumination (Doughty et al., 2019).

Finally, apart from GOME-2 sensor degradation, it would be very difficult to develop a convincing biophysical explanation as to why anomalies of GOME-2 SIF would contradict anomalies of greenness and GPP at monthly or seasonal timescales. Although short-term changes in SIF and GPP may not be congruent under certain conditions, such as stomatal closure (Marrs et al., 2020) and low or high light (Gu et al., 2019; Magney et al., 2017; Porcar-Castell et al., 2014), tower-based and satellite-based studies have instead found that the SIF/GPP correlation coefficient increases at coarser time scales (Magney et al., 2019; Yang et al., 2018a; Zhang et al., 2018c). As these studies discussed, this linearity between SIF and GPP is driven by changes in canopy leaf pigments, which determines the amount of light absorbed by canopy chlorophyll (APAR_{chl}). Therefore, we would fully expect monthly and seasonal GOME-2 SIF, GPP_{VM}, EVIn, and NDVIn to be spatially and temporally consistent as SIF and GPP are a function of chlorophyll and absorbed light ($APAR_{chl} = SIF + PQ + NPQ$).

5. Conclusions

The small anomalies we found in dry-season greenness, SIF, and photosynthesis of moist tropical forests in the Amazon during ENSO events narrows the number of potential drivers of anomalous changes in the atmospheric CO₂ growth rate during ENSO events. It is vital to characterize how drought and pluvial events affect photosynthesis of the moist tropical forests so that we can better understand and more accurately predict the effects of Earth's climate variability and human land management on atmospheric CO₂ concentrations and net carbon fluxes. Earth system models need to include variables that better track the canopy dynamics, such as leaf demography, and phenology of evergreen tropical forests (Restrepo-Coupe et al., 2017).

Our study has shown the complexity of assessing changes in dry-season greenness, SIF, and photosynthesis of tropical forests at coarse spatial resolutions (0.5 and 1.0 degree), which is to a large degree due to varying proportions of forests and other land cover types within individual gridcells. We also illustrated the potential of spaceborne GOME-2 and OCO-2 SIF data to provide new insight on photosynthetic activity in moist tropical forests, particularly during ENSO years. Frequent cloud cover and aerosols in the Amazon have limited the number of good-quality satellite observations, and coarse spatial and temporal satellite-based SIF data also significantly hinder our progress in better understanding the seasonal dynamics of SIF and its response to environmental drivers. Therefore, it is important in the future to integrate SIF data from other newly launched platforms (TROPOMI and OCO-3) and to-be-launched platforms such as FLEX and GeoCarb (Drusch et al., 2016; Polonsky et al., 2014).

Author statement

R. Doughty and X. Xiao conceived the original idea of this work. R. Doughty and X. Xiao wrote the paper. R. Doughty, Y. Qin, X. Wu, and Y. Zhang processed the data and contributed to data analysis. All authors contributed to the drafting and revision of the manuscript.

Declaration of Competing Interest

The authors declare that they have no known competing financial interests or personal relationships that could have appeared to influence the work reported in this paper.

Acknowledgements

This study was supported by research grants through the Geostationary Carbon Cycle Observatory (GeoCarb) Mission from NASA (GeoCarb Contract #80LARC17C0001), the US National Science Foundation EPSCoR Program (IIA-1301789), and the NASA Making Earth System Data Records for Use in Research Environments (MEAsURES) Program (NNN12AA01C).

Appendix A. Supplementary data

Supplementary data to this article can be found online at <https://doi.org/10.1016/j.rse.2020.112196>.

References

- Barros, F., Bittencourt, P.R., Brum, M., Restrepo-Coupe, N., Pereira, L., Teodoro, G.S., Saleska, S.R., Borma, L.S., Christoffersen, B.O., Penha, D., 2019. Hydraulic traits explain differential responses of Amazonian forests to the 2015 El Niño-induced drought. *New Phytol.* 223, 1253–1266.
- Climate Change Service, 2020. ERA5 monthly averaged data on single levels from 1979 to present. <https://doi.org/10.24381/cds.f17050d7>.
- Albert, L.P., Wu, J., Prohaska, N., Camargo, P.B., Huxman, T.E., Tribuzy, E.S., Ivanov, V. Y., Oliveira, R.S., Garcia, S., Smith, M.N., 2018. Age-dependent leaf physiology and consequences for crown-scale carbon uptake during the dry season in an Amazon evergreen forest. *New Phytologist* 219 (3), 870–884.
- Andreae, M.O., Acevedo, O.C., Araújo, A., Artaxo, P., Barbosa, C.G.G., Barbosa, H.M.J., Brito, J., Carbone, S., Chi, X., Cintra, B.B.L., 2015. The Amazon tall tower observatory (ATTO): overview of pilot measurements on ecosystem ecology, meteorology, trace gases, and aerosols. *Atmos. Chem. Phys.* 15, 10723–10776.
- Aragao, L.E.O., Malhi, Y., Roman-Cuesta, R.M., Saatchi, S., Anderson, L.O., Shimabukuro, Y.E., 2007. Spatial patterns and fire response of recent Amazonian droughts. *Geophys. Res. Lett.* 34.
- Aragao, L.E.O., Malhi, Y., Barbier, N., Lima, A., Shimabukuro, Y., Anderson, L., Saatchi, S., 2008. Interactions between rainfall, deforestation and fires during recent years in the Brazilian Amazonia. *Philosophical Transactions of the Royal Society of London B: Biological Sciences* 363, 1779–1785.
- Asner, G.P., Alencar, A., 2010. Drought impacts on the Amazon forest: the remote sensing perspective. *New Phytol.* 187, 569–578.
- Bacastow, R.B., 1976. Modulation of atmospheric carbon dioxide by the southern oscillation. *Nature* 261, 116–118.
- Betts, R.A., Jones, C.D., Knight, J.R., Keeling, R.F., Kennedy, J.J., 2016. El Niño and a record CO₂ rise. *Nat. Clim. Chang.* 6, 806–810.
- Brando, P.M., Goetz, S.J., Baccini, A., Nepstad, D.C., Beck, P.S., Christman, M.C., 2010. Seasonal and interannual variability of climate and vegetation indices across the Amazon. *Proceedings of the National Academy of Sciences* 200908741.
- Capotondi, A., Wittenberg, A.T., Newman, M., Di Lorenzo, E., Yu, J.-Y., Braconnot, P., Cole, J., Dewitte, B., Giese, B., Guilyardi, E., 2015. Understanding ENSO diversity. *Bull. Am. Meteorol. Soc.* 96, 921–938.
- Condit, R., Aguilar, S., Hernandez, A., Perez, R., Lao, S., Angher, G., Hubbell, S.P., Foster, R.B., 2004. Tropical forest dynamics across a rainfall gradient and the impact of an El Niño dry season. *J. Trop. Ecol.* 20, 51–72.
- Cui, Y., Xiao, X., Zhang, Y., Dong, J., Qin, Y., Doughty, R.B., Zhang, G., Wang, J., Wu, X., Qin, Y., Zhou, S., Joiner, J., Moore, B., 2017. Temporal consistency between gross primary production and solar-induced chlorophyll fluorescence in the ten most populous megacity areas over years. *Scientific Reports* 7. <https://doi.org/10.1038/s41598-017-13783-5>.
- Didan, K., 2015. MOD13C2 MODIS Terra Vegetation Indices Monthly L3 Global 0.05 Deg CMG V006. NASA EOSDIS Land Processes DAAC. <https://doi.org/10.5067/MODIS/MOD13C2.006>.
- Doughty, C.E., Metcalfe, D.B., Girardin, C.A.J., Amézquita, F.F., Cabrera, D.G., Huasco, W.H., Silva-Espejo, J.E., Araujo-Murakami, A., Da Costa, M.C., Rocha, W., 2015. Drought impact on forest carbon dynamics and fluxes in Amazonia. *Nature* 519, 78.
- Doughty, R., Xiao, X., Wu, X., Zhang, Y., Bajgain, R., Zhou, Y., Qin, Y., Zou, Z., McCarthy, H., Friedman, J., 2018. Responses of gross primary production of grasslands and croplands under drought, pluvial, and irrigation conditions during 2010–2016, Oklahoma, USA. *Agric. Water Manag.* 204, 47–59.
- Doughty, R., Köhler, P., Frankenberg, C., Magney, T.S., Xiao, X., Qin, Y., Wu, X., Moore, B., 2019. TROPOMI reveals dry-season increase of solar-induced chlorophyll fluorescence in the Amazon forest. *Proceedings of the National Academy of Sciences* 201908157.
- Drusch, M., Moreno, J., Del Bello, U., Franco, R., Goulas, Y., Huth, A., Kraft, S., Middleton, E.M., Miglietta, F., Mohammed, G., 2016. The fluorescence explorer mission concept—ESA's earth explorer 8. *IEEE Trans. Geosci. Remote Sens.* 55, 1273–1284.
- Ehleringer, J.R., Cerling, T.E., Helliker, B.R., 1997. C4 photosynthesis, atmospheric CO₂, and climate. *Oecologia* 112, 285–299.
- Epstein, H.E., Lauenroth, W.K., Burke, I.C., Coffin, D.P., 1997. Productivity patterns of C3 and C4 functional types in the US Great Plains. *Ecology* 78, 722–731.

- Frankenberg, C., 2015. Solar Induced Chlorophyll Fluorescence OCO-2 Lite Files (B7000) User Guide. California Institute of Technology/Jet Propulsion Laboratory.
- Frankenberg, C., Pollock, R., Lee, R.A.M., Rosenberg, R., Blavier, J.F., Crisp, D., O'Dell, C.W., Osterman, G.B., Roehl, C., Wennberg, P.O., 2014. The orbiting carbon observatory (OCO-2): spectrometer performance evaluation using pre-launch direct sun measurements. *Atmospheric Measurement Techniques Discussions* 7.
- Galvão, L.S., dos Santos, J.R., Roberts, D.A., Breunig, F.M., Toomey, M., de Moura, Y.M., 2011. On intra-annual EVI variability in the dry season of tropical forest: a case study with MODIS and hyperspectral data. *Remote Sens. Environ.* 115, 2350–2359.
- Gao, B.-C., 1996. NDWI—A normalized difference water index for remote sensing of vegetation liquid water from space. *Remote Sens. Environ.* 58, 257–266.
- Gatti, L.V., Gloor, M., Miller, J.B., Doughty, C.E., Malhi, Y., Domingues, L.G., Basso, L.S., Martinewski, A., Correia, C.S.C., Borges, V.F., 2014. Drought sensitivity of Amazonian carbon balance revealed by atmospheric measurements. *Nature* 506, 76.
- Gloor, E., Wilson, C., Chipperfield, M.P., Chevallier, F., Buermann, W., Boesch, H., Parker, R., Somkuti, P., Gatti, L.V., Correia, C., 2018. Tropical land carbon cycle responses to 2015/16 El Niño as recorded by atmospheric greenhouse gas and remote sensing data. *Philosophical Transactions of the Royal Society B: Biological Sciences* 373, 20170302.
- Gonçalves, N.B., Lopes, A.P., Dalagnol, R., Wu, J., Pinho, D.M., Nelson, B.W., 2020. Both near-surface and satellite remote sensing confirm drought legacy effect on tropical forest leaf phenology after 2015/2016 ENSO drought. *Remote Sens. Environ.* 237, 111489.
- Graham, E.A., Mulkey, S.S., Kitajima, K., Phillips, N.G., Wright, S.J., 2003. Cloud cover limits net CO₂ uptake and growth of a rainforest tree during tropical rainy seasons. *Proc. Natl. Acad. Sci.* 100, 572–576.
- Gu, L., Han, J., Wood, J.D., Chang, C.Y.-Y., Sun, Y., 2019. Sun-induced Chl fluorescence and its importance for biophysical modeling of photosynthesis based on light reactions. *New Phytol.* 223, 1179–1191.
- Guan, K., Pan, M., Li, H., Wolf, A., Wu, J., Medvigy, D., Caylor, K.K., Sheffield, J., Wood, E.F., Malhi, Y., 2015. Photosynthetic seasonality of global tropical forests constrained by hydroclimate. *Nat. Geosci.* 8, 284.
- Guanter, L., Aben, I., Tol, P., Krijger, J.M., Hollstein, A., Köhler, P., Damm, A., Joiner, J., Frankenberg, C., Landgraf, J., 2015. Potential of the TROPospheric monitoring instrument (TROPOMI) onboard the Sentinel-5 precursor for the monitoring of terrestrial chlorophyll fluorescence. *Atmospheric Measurement Techniques* 8, 1337–1352.
- Haxeltine, A., Prentice, I.C., 1996. A general model for the light-use efficiency of primary production. *Funct. Ecol.* 551–561.
- Hilker, T., Lyapustin, A.I., Hall, F.G., Myneni, R., Knyazikhin, Y., Wang, Y., Tucker, C.J., Sellers, P.J., 2015. On the measurability of change in Amazon vegetation from MODIS. *Remote Sens. Environ.* 166, 233–242.
- Hubau, W., Lewis, S.L., Phillips, O.L., Affum-Baffoe, K., Beckman, H., Cuni-Sanchez, A., Daniels, A.K., Kwango, C.E.N., Fauset, S., Mukinzi, J.M., 2020. Asynchronous Carbon Sink Saturation in African and Amazonian Tropical Forests.
- Huete, A., Didan, K., Miura, T., Rodriguez, E.P., Gao, X., Ferreira, L.G., 2002. Overview of the radiometric and biophysical performance of the MODIS vegetation indices. *Remote Sens. Environ.* 83, 195–213.
- Huete, A.R., Didan, K., Shimabukuro, Y.E., Ratana, P., Saleska, S.R., Hutrya, L.R., Yang, W., Nemani, R.R., Myneni, R., 2006. Amazon rainforests green-up with sunlight in dry season. *Geophys. Res. Lett.* 33.
- Huffman, G.J., Bolvin, D.T., Nelkin, E.J., Wolff, D.B., Adler, R.F., Gu, G., Hong, Y., Bowman, K.P., Stocker, E.F., 2007. The TRMM multisatellite precipitation analysis (TMPA): quasi-global, multiyear, combined-sensor precipitation estimates at fine scales. *J. Hydrometeorol.* 8, 38–55.
- Huffman, G.J., Stocker, E.F., Bolvin, D.T., Nelkin, E.J., 2014. 3B43: Multisatellite Precipitation. NASA/GSFC, Greenbelt, MD, USA. <https://doi.org/10.5067/TRMM/TMPA/MONTH/7>.
- Jimenez, J.C., Libonati, R., Peres, L.F., 2018. Droughts over Amazonia in 2005, 2010, and 2015: a cloud cover perspective. *Front. Earth Sci.* 6, 227.
- Jiménez-Muñoz, J.C., Mattar, C., Barichivich, J., Santamaría-Artigas, A., Takahashi, K., Malhi, Y., Sobrino, J.A., Van Der Schrier, G., 2016. Record-breaking warming and extreme drought in the Amazon rainforest during the course of El Niño 2015–2016. *Sci. Rep.* 6, 33130.
- Joiner, J., Guanter, L., Lindstrot, R., Voigt, M., Vasilkov, A.P., Middleton, E.M., Huemmrich, K.F., Yoshida, Y., Frankenberg, C., 2013. Global monitoring of terrestrial chlorophyll fluorescence from moderate-spectral-resolution near-infrared satellite measurements: methodology, simulations, and application to GOME-2. *Atmospheric Measurement Techniques* 6, 2803–2823.
- Joiner, J., Yoshida, Y., Guanter, L., Middleton, E.M., 2016. New methods for the retrieval of chlorophyll red fluorescence from hyperspectral satellite instruments: simulations and application to GOME-2 and SCIAMACHY. *Atmos. Meas. Tech.* 9, 3939–3967. <https://doi.org/10.5194/amt-9-3939-2016>.
- Keeling, C.D., Revelle, R., 1985. Effects of El Niño/southern oscillation on the atmospheric content of carbon dioxide. *Meteoritics* 20, 437–450.
- Keeling, C.D., Whorf, T.P., Wahlen, M., Van der Plicht, J., 1995. Interannual extremes in the rate of rise of atmospheric carbon dioxide since 1980. *Nature* 375, 666–670.
- Keller, M., Alencar, A., Asner, G.P., Braswell, B., Bustamante, M., Davidson, E., Feldpausch, T., Fernandes, E., Goulden, M., Kabat, P., 2004. Ecological research in the large-scale biosphere-atmosphere experiment in Amazonia: early results. *Ecol. Appl.* 14, 3–16.
- Koren, G., van Schaik, E., Araújo, A.C., Boersma, K.F., Gärtner, A., Killaars, L., Kooreman, M.L., Kruij, B., van der Laan-Luijckx, I.T., von Randow, C., 2018. Widespread reduction in sun-induced fluorescence from the Amazon during the 2015/2016 El Niño. *Philosophical Transactions of the Royal Society B: Biological Sciences* 373, 20170408.
- Laurance, W.F., Williamson, G.B., 2001. Positive feedbacks among forest fragmentation, drought, and climate change in the Amazon. *Conserv. Biol.* 15, 1529–1535.
- Lee, J.-E., Frankenberg, C., van der Tol, C., Berry, J.A., Guanter, L., Boyce, C.K., Fisher, J.B., Morrow, E., Worden, J.R., Asefi, S., 2013. Forest productivity and water stress in Amazonia: observations from GOSAT chlorophyll fluorescence. *Proc. R. Soc. Lond. B Biol. Sci.* 280, 20130171.
- Lewis, S.L., Brando, P.M., Phillips, O.L., van der Heijden, G.M., Nepstad, D., 2011. The 2010 Amazon drought. *Science* 331, 554–554.
- Li, X., Xiao, J., He, B., Altaf Arain, M., Beringer, J., Desai, A.R., Emmel, C., Hollinger, D. Y., Krasnova, A., Mammarella, I., 2018. Solar-induced chlorophyll fluorescence is strongly correlated with terrestrial photosynthesis for a wide variety of biomes: first global analysis based on OCO-2 and flux tower observations. *Glob. Chang. Biol.* 24, 3990–4008.
- Liu, J., Bowman, K.W., Schimel, D.S., Parazoo, N.C., Jiang, Z., Lee, M., Bloom, A.A., Wunch, D., Frankenberg, C., Sun, Y., 2017. Contrasting carbon cycle responses of the tropical continents to the 2015–2016 El Niño. *Science* 358, eaam5690.
- Lopes, A.P., Nelson, B.W., Wu, J., de Alencastro Graça, P.M.L., Tavares, J.V., Prohaska, N., Martins, G.A., Saleska, S.R., 2016. Leaf flush drives dry season green-up of the Central Amazon. *Remote Sens. Environ.* 182, 90–98.
- Ma, J., Xiao, X., Zhang, Y., Doughty, R., Chen, B., Zhao, B., 2018. Spatial-temporal consistency between gross primary productivity and solar-induced chlorophyll fluorescence of vegetation in China during 2007–2014. *Sci. Total Environ.* 639, 1241–1253.
- Maeda, E.E., Heiskanen, J., Aragão, L.E., Rinne, J., 2014. Can MODIS EVI monitor ecosystem productivity in the Amazon rainforest? *Geophys. Res. Lett.* 41, 7176–7183.
- Maeda, E.E., Moura, Y.M., Wagner, F., Hilker, T., Lyapustin, A.I., Wang, Y., Chave, J., Möttöus, M., Aragão, L.E., Shimabukuro, Y., 2016. Consistency of vegetation index seasonality across the Amazon rainforest. *Int. J. Appl. Earth Obs. Geoinf.* 52, 42–53.
- Magney, T.S., Frankenberg, C., Fisher, J.B., Sun, Y., North, G.B., Davis, T.S., Kornfeld, A., Siebke, K., 2017. Connecting active to passive fluorescence with photosynthesis: a method for evaluating remote sensing measurements of Chl fluorescence. *New Phytol.* 215, 1594–1608.
- Magney, T.S., Bowling, D.R., Logan, B.A., Grossmann, K., Stutz, J., Blanken, P.D., Burns, S.P., Cheng, R., Garcia, M.A., Köhler, P., 2019. Mechanistic evidence for tracking the seasonality of photosynthesis with solar-induced fluorescence. *Proc. Natl. Acad. Sci.* 116, 11640–11645.
- Marengo, J.A., Nobre, C.A., Tomasella, J., Oyama, M.D., Sampaio de Oliveira, G., De Oliveira, R., Carmo, H., Alves, L.M., Brown, I.F., 2008. The drought of Amazonia in 2005. *J. Clim.* 21, 495–516.
- Marengo, J.A., Tomasella, J., Alves, L.M., Soares, W.R., Rodriguez, D.A., 2011. The drought of 2010 in the context of historical droughts in the Amazon region. *Geophys. Res. Lett.* 38.
- Marrs, J.K., Reblin, J.S., Logan, B.A., Allen, D.W., Reinmann, A.B., Bombard, D.M., Tabachnik, D., Hutrya, L.R., 2020. Solar-induced fluorescence does not track photosynthetic carbon assimilation following induced stomatal closure. *Geophysical Research Letters* 47 (e2020GL087956).
- Morton, D.C., Nagol, J., Carabjal, C.C., Rosette, J., Palace, M., Cook, B.D., Vermote, E.F., Harding, D.J., North, P.R., 2014. Amazon forests maintain consistent canopy structure and greenness during the dry season. *Nature* 506, 221.
- Nepstad, D.C., de Carvalho, C.R., Davidson, E.A., Jipp, P.H., Lefebvre, P.A., Negreiros, G. H., da Silva, E.D., Stone, T.A., Trumbore, S.E., Vieira, S., 1994. The role of deep roots in the hydrological and carbon cycles of Amazonian forests and pastures. *Nature* 372, 666.
- Nepstad, D.C., Tohver, I.M., Ray, D., Moutinho, P., Cardinot, G., 2007. Mortality of large trees and lianas following experimental drought in an Amazon forest. *Ecology* 88, 2259–2269.
- Phillips, O.L., Aragão, L.E., Lewis, S.L., Fisher, J.B., Lloyd, J., López-González, G., Malhi, Y., Monteagudo, A., Peacock, J., Quesada, C.A., 2009. Drought sensitivity of the Amazon rainforest. *Science* 323, 1344–1347.
- Polonsky, I.N., O'Brien, D.M., Kumer, J.B., O'Dell, C.W., 2014. Performance of a geostationary mission, geoCARB, to measure CO₂, CH₄ and CO column-averaged concentrations. *Atmospheric Measurement Techniques* 7, 959–981.
- Porcar-Castell, A., Tyystjärvi, E., Atherton, J., Van der Tol, C., Flexas, J., Pfundel, E.E., Moreno, J., Frankenberg, C., Berry, J.A., 2014. Linking chlorophyll a fluorescence to photosynthesis for remote sensing applications: mechanisms and challenges. *J. Exp. Bot.* 65, 4065–4095.
- Qin, Y., Xiao, X., Dong, J., Zhang, Y., Wu, X., Shimabukuro, Y., Arai, E., Biradar, C., Wang, J., Zou, Z., 2019. Improved estimates of forest cover and loss in the Brazilian Amazon in 2000–2017. *Nature Sustainability* 1.
- Qin, Y., Xiao, X., Dong, J., Zhang, G., Roy, P.S., Joshi, P.K., Gilani, H., Murthy, M.S.R., Jin, C., Wang, J., 2016. Mapping forests in monsoon Asia with ALOS PALSAR 50-m mosaic images and MODIS imagery in 2010. *Sci. Rep.* 6, 20880.
- Restrepo-Coupe, N., da Rocha, H.R., Hutrya, L.R., da Araujo, A.C., Borma, L.S., Christoffersen, B., Cabral, O.M., de Camargo, P.B., Cardoso, F.L., da Costa, A.C.L., 2013. What drives the seasonality of photosynthesis across the Amazon basin? A cross-site analysis of eddy flux tower measurements from the Brasil flux network. *Agric. For. Meteorol.* 182, 128–144.
- Restrepo-Coupe, N., Levine, N.M., Christoffersen, B.O., Albert, L.P., Wu, J., Costa, M.H., Galbraith, D., Imbuzeiro, H., Martins, G., da Araujo, A.C., 2017. Do dynamic global vegetation models capture the seasonality of carbon fluxes in the Amazon basin? A data-model intercomparison. *Glob. Chang. Biol.* 23, 191–208.
- Rice, A.H., Pyle, E.H., Saleska, S.R., Hutrya, L., Palace, M., Keller, M., De Camargo, P.B., Portillo, K., Marques, D.F., Wofsy, S.C., 2004. Carbon balance and vegetation dynamics in an old-growth Amazonian forest. *Ecol. Appl.* 14, 55–71.

- Rivera, G., Elliott, S., Caldas, L.S., Nicolossi, G., Coradin, V.T., Borchert, R., 2002. Increasing day-length induces spring flushing of tropical dry forest trees in the absence of rain. *Trees* 16, 445–456.
- Saatchi, S., Asefi-Najafabady, S., Malhi, Y., Aragão, L.E., Anderson, L.O., Myneni, R.B., Nemani, R., 2013. Persistent effects of a severe drought on Amazonian forest canopy. *Proc. Natl. Acad. Sci.* 110, 565–570.
- Saleska, S.R., Miller, S.D., Matross, D.M., Goulden, M.L., Wofsy, S.C., Da Rocha, H.R., De Camargo, P.B., Crill, P., Daube, B.C., De Freitas, H.C., 2003. Carbon in Amazon forests: unexpected seasonal fluxes and disturbance-induced losses. *Science* 302, 1554–1557.
- Saleska, S.R., Didan, K., Huete, A.R., Da Rocha, H.R., 2007. Amazon forests green-up during 2005 drought. *Science* 318, 612.
- Saleska, S.R., Wu, J., Guan, K., Araujo, A.C., Huete, A., Nobre, A.D., Restrepo-Coupe, N., 2016. Dry-season greening of Amazon forests. *Nature* 531, E4.
- Samanta, A., Ganguly, S., Hashimoto, H., Devadiga, S., Vermote, E., Knyazikhin, Y., Nemani, R.R., Myneni, R.B., 2010. Amazon forests did not green-up during the 2005 drought. *Geophys. Res. Lett.* 37.
- Santoso, A., McPhaden, M.J., Cai, W., 2017. The defining characteristics of ENSO extremes and the strong 2015/2016 El Niño. *Rev. Geophys.* 55, 1079–1129.
- Sun, Y., Frankenberg, C., Jung, M., Joiner, J., Guanter, L., Köhler, P., Magney, T., 2018. Overview of solar-induced chlorophyll fluorescence (SIF) from the orbiting carbon Observatory-2: retrieval, cross-mission comparison, and global monitoring for GPP. *Remote Sens. Environ.* 209, 808–823.
- Vermote, E., 2015. MOD09A1 MODIS/Terra surface reflectance 8-day L3 global 500m SIN grid V006. NASA EOSDIS Land Processes DAAC. <https://doi.org/10.5067/MODIS/MOD09A1.006>.
- Wagner, F.H., Hérault, B., Rossi, V., Hilker, T., Maeda, E.E., Sanchez, A., Lyapustin, A.I., Galvão, L.S., Wang, Y., Aragão, L.E., 2017. Climate drivers of the Amazon forest greening. *PLoS One* 12, e0180932.
- Wolter, K., Timlin, M.S., 2011. El Niño/southern oscillation behaviour since 1871 as diagnosed in an extended multivariate ENSO index (MEI. Ext). *Int. J. Climatol.* 31, 1074–1087.
- Wright, S.J., Van Schaik, C.P., 1994. Light and the phenology of tropical trees. *Am. Nat.* 143, 192–199.
- Wu, J., Albert, L.P., Lopes, A.P., Restrepo-Coupe, N., Hayek, M., Wiedemann, K.T., Guan, K., Stark, S.C., Christoffersen, B., Prohaska, N., 2016. Leaf development and demography explain photosynthetic seasonality in Amazon evergreen forests. *Science* 351, 972–976.
- Wu, J., Kobayashi, H., Stark, S.C., Meng, R., Guan, K., Tran, N.N., Gao, S., Yang, W., Restrepo-Coupe, N., Miura, T., 2018. Biological processes dominate seasonality of remotely sensed canopy greenness in an Amazon evergreen forest. *New Phytol.* 217, 1507–1520.
- Xiao, X., Boles, S., Frohling, S., Salas, W., Moore Iii, B., Li, C., He, L., Zhao, R., 2002. Observation of flooding and rice transplanting of paddy rice fields at the site to landscape scales in China using VEGETATION sensor data. *Int. J. Remote Sens.* 23, 3009–3022.
- Xiao, X., Zhang, Q., Braswell, B., Urbanski, S., Boles, S., Wofsy, S., Moore, B., Ojima, D., 2004. Modeling gross primary production of temperate deciduous broadleaf forest using satellite images and climate data. *Remote Sens. Environ.* 91, 256–270.
- Xiao, X., Zhang, Q., Saleska, S., Huttyra, L., De Camargo, P., Wofsy, S., Frohling, S., Boles, S., Keller, M., Moore, B., 2005. Satellite-based modeling of gross primary production in a seasonally moist tropical evergreen forest. *Remote Sens. Environ.* 94, 105–122.
- Xiao, X., Hagen, S., Zhang, Q., Keller, M., Moore III, B., 2006. Detecting leaf phenology of seasonally moist tropical forests in South America with multi-temporal MODIS images. *Remote Sens. Environ.* 103, 465–473.
- Xin, F., Xiao, X., Zhao, B., Miyata, A., Baldocchi, D., Knox, S., Kang, M., Shim, K., Min, S., Chen, B., 2017. Modeling gross primary production of paddy rice cropland through analyses of data from CO₂ eddy flux tower sites and MODIS images. *Remote Sens. Environ.* 190, 42–55.
- Xu, L., Samanta, A., Costa, M.H., Ganguly, S., Nemani, R.R., Myneni, R.B., 2011. Widespread decline in greenness of Amazonian vegetation due to the 2010 drought. *Geophys. Res. Lett.* 38.
- Yang, K., Ryu, Y., Dechant, B., Berry, J.A., Hwang, Y., Jiang, C., Kang, M., Kim, J., Kimm, H., Kornfeld, A., 2018a. Sun-induced chlorophyll fluorescence is more strongly related to absorbed light than to photosynthesis at half-hourly resolution in a rice paddy. *Remote Sens. Environ.* 216, 658–673.
- Yang, J., Tian, H., Pan, S., Chen, G., Zhang, B., Dangal, S., 2018b. Amazon drought and forest response: largely reduced forest photosynthesis but slightly increased canopy greenness during the extreme drought of 2015/2016. *Glob. Chang. Biol.* 24, 1919–1934.
- Zhang, Y., Joiner, J., Gentine, P., Zhou, S., 2018. Reduced solar-induced chlorophyll fluorescence from GOME-2 during Amazon drought caused by dataset artifacts. *Glob. Chang. Biol.* 24, 2229–2230.
- Zhang, Yao, Xiao, X., Jin, C., Dong, J., Zhou, S., Wagle, P., Joiner, J., Guanter, L., Zhang, Yongguang, Zhang, G., 2016. Consistency between sun-induced chlorophyll fluorescence and gross primary production of vegetation in North America. *Remote Sens. Environ.* 183, 154–169.
- Zhang, Y., Xiao, X., Wolf, S., Wu, J., Wu, X., Gioli, B., Wohlfahrt, G., Cescatti, A., van der Tol, C., Zhou, S., 2018. Spatio-temporal convergence of maximum daily light-use efficiency based on radiation absorption by canopy chlorophyll. *Geophys. Res. Lett.* 45, 3508–3519.
- Zhang, Y., Xiao, X., Wu, X., Zhou, S., Zhang, G., Qin, Y., Dong, J., 2017. A global moderate resolution dataset of gross primary production of vegetation for 2000–2016. *Scientific Data* 4, 170165.
- Zhang, Yao, Xiao, X., Zhang, Yongguang, Wolf, S., Zhou, S., Joiner, J., Guanter, L., Verma, M., Sun, Y., Yang, X., 2018c. On the relationship between sub-daily instantaneous and daily total gross primary production: implications for interpreting satellite-based SIF retrievals. *Remote Sens. Environ.* 205, 276–289.
- Zhao, M., Heinsch, F.A., Nemani, R.R., Running, S.W., 2005. Improvements of the MODIS terrestrial gross and net primary production global data set. *Remote Sens. Environ.* 95, 164–176.